Control of matter-wave superradiance with a high-finesse ring cavity

S. Bux,[1] H. Tomczyk,[1] D. Schmidt,[1] Ph. W. Courteille,[2] N. Piovella,[3] and C. Zimmermann[1,*]

[1]*Physikalisches Institut, Eberhard-Karls-Universität Tübingen, Auf der Morgenstelle 14, D-72076 Tübingen, Germany*

[2]*Instituto de Física de São Carlos, Universidade de São Paulo, 13560-970 São Carlos, SP, Brazil*

[3]*Dipartimento di Fisica, Università degli Studi di Milano, Via Celoria 16, I-20133 Milano, Italy*

(Received 10 December 2012; published 6 February 2013)

We experimentally investigate light scattering from a Bose-Einstein condensate which is positioned inside an optical ring cavity. With a cavity linewidth at the recoil limit, the resulting superradiant scattering behavior is strongly influenced by the cavity detuning. The experimental observations are interpreted with a quantum mean-field description and with a rate-equation model. We discuss applications in the context of quantum phase transitions, Dicke subradiance, and nonconventional superfluidity.

DOI: 10.1103/PhysRevA.87.023607 PACS number(s): 03.75.Lm, 37.30.+i, 05.65.+b

I. INTRODUCTION

In recent years, the collective behavior of atoms inside an optical resonator has been investigated in a number of experiments with cold thermal clouds [1–3] and with Bose-Einstein condensates [4–6]. In these experiments the atoms all interact with the same optical mode, which may be interpreted as an effective long-range interaction between the atoms (in the context of atomic clouds in optical cavities; see, for instance, [7]). This leads to collectively excited states which are closely related to quantum phase transitions and dynamical instabilities [4,8]. From a different perspective, atom-cavity combinations turn out to be useful model systems for investigating collective scattering phenomena such as matter-wave superradiance [4] and coherent atomic recoil lasing (CARL) [3,9]. Cavity-enhanced Rayleigh scattering has also been proposed to nondestructively observe correlations in quantum gases [10]. Finally, the resonator can be exploited to cool atomic and molecular ensembles even below the recoil limit [6,11].

Typically, the atom-cavity system is pumped by coupling light through one of the cavity mirrors. However, in recent experiments the atoms have also been irradiated with an external light beam such that the initially empty resonator fills with photons due to Rayleigh scattering of the pump light by the atoms. By pumping a standing-wave resonator with an external standing wave, the Dicke quantum phase transition has recently been observed [12]. For high-quality mirrors and sufficiently large mirror separations, the cavity linewidth can be reduced below the recoil frequency shift which a photon acquires if it is scattered from an atom. Thus, by tuning the cavity relative to the frequency of the scattered photons, scattering from specific atomic momentum states can be suppressed or enhanced [13]. In principle, this allows for tailoring novel scenarios where only a few momentum states dominate the dynamics [6]. Matter-wave subradiance has recently been proposed in such a system [14]. Furthermore, the atoms can be stabilized this way against excitation into higher-momentum states.

In this paper we analyze in some detail our recent experiment with a high-finesse ring cavity which is pumped by scattering photons from an external traveling wave into the ring cavity [13]. In contrast to a standing-wave resonator, the ring geometry offers two propagating light modes to which the atoms can couple. Consequently, two different recoil momenta are transferred to the atoms depending on the direction the scattered photon travels inside the resonator. As a consequence, a Bose-Einstein condensate, initially at rest, fragments into a series of momentum states and forms a rectangular lattice in momentum space. This is similar to the well-known key experiment on matter-wave superradiance at MIT [15,16], however, with the difference that at MIT no cavity was used and the direction of scattering was determined by the shape of the condensate. In Secs. II and III we introduce the experimental scenario and discuss two models that can be derived from the full quantum equations. A mean-field model, which neglects quantum fluctuations, describes the complex dynamics of the experiment reasonably well but does not allow for a simple intuitive interpretation. However, it turns out that efficient control of matter-wave superradiance by the cavity is only possible for low pump intensities and consequently weak coupling between the atoms and the light. In this regime the mean-field model can be approximated by a rate-equation model, which suggests a very simple picture of the underlying physics. This is the first result of the paper. In Sec. IV we compare the theoretical models with the experimental observations and find that the current experiment has been carried out in a regime where the pump intensity is too strong for efficient control of superradiance. This will be possible only for reduced pump intensities and longer pump times. This is the second result of the paper. We close the paper with a discussion and an outlook in Sec. V.

II. EXPERIMENT

The experimental setup has been described in detail in Ref. [13]. In short, we generate a ^{87}Rb Bose-Einstein condensate (BEC) in a Ioffe-type magnetic trap and transfer it into the mode focus of a 87-mm-long ring cavity with a finesse of $F = 130\,000$. The plane of the resonator is oriented perpendicular to gravity. The focus of the TEM_{00} mode at the position of the atoms has a slightly elliptical cross section with beam radii of $w_x = 88\ \mu$m (horizontal) and $w_y = 117\ \mu$m (vertical), resulting in a mode volume of $V = 1/2L\pi w_x w_y = 1.37\ \mathrm{mm}^3$. The cavity-to-free-space scattering ratio (Purcell factor) amounts

*clz@pit.physik.uni-tuebingen.de

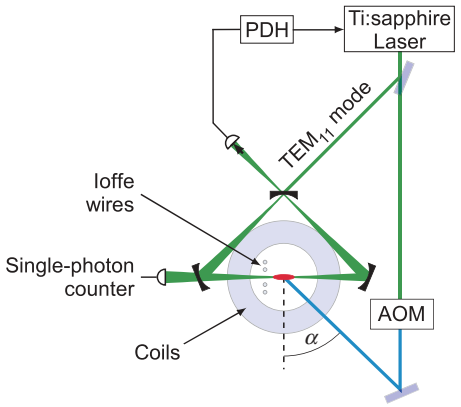

FIG. 1. (Color online) Geometry of the experiment: A BEC is created in a Ioffe-Pritchard trap and then placed in the waist of a TEM_{11} mode of an optical ring cavity (green). A pump beam is irradiated from the side under the angle $\alpha = 37^\circ$. A single-photon counter records the photons transmitted through one of the cavity mirrors.

to $\eta = 6F/(\pi k^2 w_x w_y) = 0.38$ [17]. The half-line width of the cavity is identical to the amplitude decay rate $\kappa_c = 2\pi \times 13.0$ kHz and slightly smaller than the two-photon recoil shift for rubidium of $\omega_{\rm rec} = 2\pi \times 14.4$ kHz. The symmetry axis of the cigar-shaped BEC is oriented parallel to the optical axis of the cavity and to the magnetic field of the trap at the position of the condensate. The BEC is irradiated with a linearly polarized external pump laser beam with its wave vector **k** lying in the plane of the ring cavity at an angle of $\alpha = 37^\circ$ relative to the normal of the cavity's optical axis (see Fig. 1). The polarization of the pump light is oriented normal to the plane of the cavity, and its intensity typically amounts to several 10 mW/cm^2. A two-mode offset locking scheme [18] controls the detuning Δ_c between the pump laser and the resonance of the empty cavity with a precision of about 100 Hz, which is by far sufficient to resolve the cavity resonance line. The detuning Δ_a of the pump laser relative to the rubidium D_1 line ($F = 2 \rightarrow F' = 2$) is chosen in the range of a few gigahertz. The experimental observations turned out to be independent of the sign of the detuning (see also Figs. 6 and 7 below and [19]).

After a variable pump duration τ of typically 200 μs the pump laser is turned off, and the BEC is released from the trap. After 15 ms of ballistic expansion an absorption image is taken. It shows the momentum distribution of the atoms inside the trap at the time when the pump beam is turned off. The light that the atoms scatter into the left running cavity mode is observed by counting the photons that are transmitted through one of the cavity mirrors.

When the frequency of the incident pump light is far detuned from a resonance of the cavity or when its polarization is chosen parallel to the cavity plane (p polarization), no modification of the condensate's momentum distribution is observed, and no photons are counted. However, when the pump frequency is close to a cavity resonance and for s polarization, the absorption image shows a rectangular pattern according to a discrete superposition of specific momentum states [Fig. 2(b)]. At the same time, a large number of photons are scattered into the cavity [Fig. 2(a)]. In the experiment, the detuning Δ_c, the pump intensity I, and pump duration τ are varied, and the relative numbers of atoms in the different momentum states are derived from the recorded images.

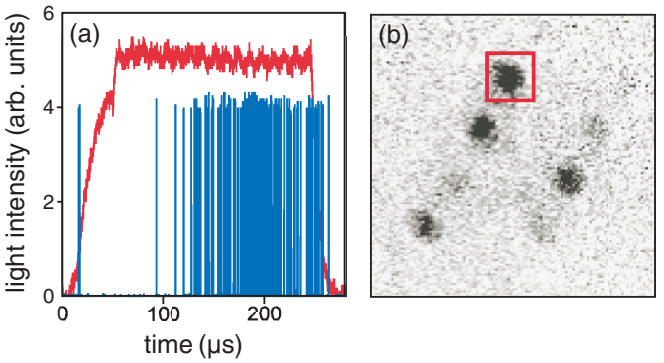

FIG. 2. (Color online) Main signatures of the experiment. (a) A single-photon detector counts the photons which are scattered into the left running cavity mode and leak out through one of the high-reflectivity mirrors. The red (light gray) line indicates the power of the pump beam in arbitrary units. The blue (dark gray) spikes represent single-photon counts. (b) Atomic momentum distribution observed via time-of-flight absorption imaging. The populations in the individual momentum states are obtained by summing the pixel values in a fixed area (red rectangle).

III. THEORETICAL DESCRIPTION

The theoretical description is based on Ref. [20]. The atomic condensate is initially at rest. An incident pump photon with wave vector k_p is scattered by an atom into one of the two cavity modes with wave vectors k_1 or k_2 (see Fig. 3), and the atom acquires a corresponding momentum kick. Subsequent scattering of photons leads to a spreading of the atoms over a rectangular lattice in momentum space. The momentum states can be labeled by the number of photons m and n an atom has scattered into the right- and left-propagating cavity modes, respectively (see Fig. 1). A specific momentum transition is related to a specific frequency shift of the scattered photons. Depending on the detuning of the photon frequency relative to the resonance of the cavity, the transition can thus be enhanced or suppressed.

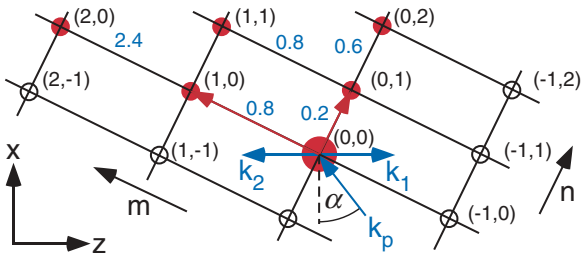

FIG. 3. (Color online) Momentum space accessible to the atoms. An incident pump photon with wave vector k_p is scattered by an atom into one of the two cavity modes with wave vectors k_1 or k_2. Due to the discrete momentum transfer during scattering the possible atomic momentum states (m,n) form a rectangular lattice in momentum space. The blue (gray) numbers indicate the negative recoil frequency shift of the scattered photon in units of the two-photon recoil frequency of 14.4 kHz. The states with open circles are occupied if photons are scattered from the cavity into the pump beam.

Photons which circulate inside the resonator can also be scattered by the atoms back into the pump beam with significant probability. By this process, momentum states with negative quantum numbers m and n may be occupied (open circles in Fig. 3). Finally, photons can be scattered between the forward- and the backward-propagating cavity modes (cross-cavity-mode scattering). This changes m and n simultaneously by one unit but with opposite sign. Recoil heating caused by scattering into free space is neglected in our analysis.

Since the atomic motion takes place in the plane of the ring cavity, each atom is described by two noncommuting position and momentum variables. Depending on the direction into which a photon has been scattered, two different recoil momenta can be imparted to an atom, $\hbar\mathbf{q}_{1,2} = \hbar k_p[\mathbf{e}_x \cos\alpha - \mathbf{e}_z(\sin\alpha \pm 1)]$; see Fig. 3. We chose a coordinate system generated by the unity vectors

$$\mathbf{e}_{1,2} \equiv \frac{1}{\sqrt{2}}\left(\mathbf{e}_x \frac{\cos\alpha}{\sqrt{1 \pm \sin\alpha}} \mp \mathbf{e}_z\sqrt{1 \pm \sin\alpha}\right). \tag{1}$$

In this coordinate system the momentum $\mathbf{p} = p_1\mathbf{e}_1 + p_2\mathbf{e}_2$ of an atom is given by the two normalized momentum variables $P_\mu = p_\mu/\hbar q_\mu$, with $\mu = 1,2$. The atomic position $\mathbf{x} = x_1\mathbf{e}_1 + x_2\mathbf{e}_2$ is encoded in the two phases $\theta_\mu = x_\mu q_\mu$. Treating the atomic motion as being quantized, the commutation rule can be written $[\hat\theta_{\mu,j}, \hat P_{\nu,m}] = i\delta_{\mu,\nu}\delta_{j,m}$, with $j,m = 1,\ldots,N$.The annihilation and creation operators for the cavity modes satisfy $[\hat a_\mu, \hat a_\nu^\dagger] = \delta_{\mu,\nu}$. The many-particle Hamiltonian $\hat H = \sum_{j=1}^N \hat h_j$ then explicitly reads

$$\begin{aligned}\hat H = &\sum_{j=1}^{N} \omega_{r1}\hat P_{1j}^2 + \omega_{r2}\hat P_{2j}^2 + i\frac{g\Omega}{2\Delta_a}\left[\hat a_1^\dagger e^{i\hat\theta_{1j}} + \hat a_2^\dagger e^{i\hat\theta_{2j}} - \text{H.c.}\right]\\ &+ \frac{g^2}{\Delta_a}[\hat a_1\hat a_2^\dagger e^{i(\hat\theta_{2j} - \hat\theta_{1j})} + \text{H.c.}]\\ &- \left(\Delta_c - \frac{Ng^2}{\Delta_a}\right)(\hat a_1^\dagger\hat a_1 + \hat a_2^\dagger\hat a_2).\end{aligned} \tag{2}$$

Here, $\omega_{r1,2} = \frac{1}{2}\omega_{\text{rec}}(1 \pm \sin\alpha)$ is the projection of ω_{rec} onto the two cavity modes. The coupling strength between the cavity modes and the atomic motion is given by $g\Omega/(2\Delta_a)$, with the atom-cavity coupling strength $g = \sqrt{\frac{d_{\text{eff}}^2\omega}{2\epsilon_0\hbar V}} = 2\pi \times 48.9$ kHz (which is equivalent to half the single-photon Rabi frequency) and the Rabi frequency due to the pump beam $\Omega = d_{\text{eff}}E_p/\hbar = 2\pi \times 1.514\ \text{MHz}\sqrt{I_p\ \text{cm}^2/\ \text{mW}}$. E_p is the rms electric field of the pump beam at the position of the atoms. It is related to the pump intensity by $E_p = \sqrt{\frac{2I_p}{c\epsilon_0}} = 87.0\ \text{V/ m}\sqrt{I_p\ \text{cm}^2/\ \text{mW}}$. The effective dipole matrix element d_{eff} contains the matrix elements $d_1 := -\sqrt{\frac{1}{6}}d$ and $d_2 := \sqrt{\frac{1}{2}}d$ of the two σ^- transitions ($F = 2, m_F = 2 \to F = 1, m_F = 1$; $F = 2, m_F = 2 \to F = 2, m_F = 1$), which are driven by a field with linear polarization normal to the quantization axis. The quantization axis is set parallel to the optical axis of the cavity. The reduced matrix element $d = \langle J = 1/2\,||er||\,J' = 1/2\rangle = 2.537 \times 10^{-29}$ C m, and the roots are the Clebsch-Gordon coefficients. The difference between the resonance frequencies of the two transitions of 812 MHz leads to a negligible correction of below 5%. An additional factor of $\frac{1}{2}$ takes care of the fact that only one circular component of the linearly polarized light field couples to the σ^- transitions. Thus $d_{\text{eff}} = \frac{1}{2}\sqrt{d_1^2 + d_2^2} = 0.408d$. The detuning of the pump frequency ω_p from the resonance frequency ω_0 of the D_1 line of ^{87}Rb is $\Delta_a = \omega_p - \omega_0$.

In the second quantized representation of the particle field the many-body Hamiltonian reads

$$\begin{aligned}\hat H_{\text{sq}} = &\int_0^{2\pi} d\theta_1 \int_0^{2\pi} d\theta_2 \hat\Psi^\dagger(\theta_1,\theta_2)\hat h(\theta_1,\theta_2, -i\partial_{\theta_1},\\ &-i\partial_{\theta_2}, a_1, a_1^\dagger, a_2, a_2^\dagger)\hat\Psi(\theta_1,\theta_2).\end{aligned} \tag{3}$$

The field operators have to satisfy the commutation relations $[\hat\Psi(\theta_1,\theta_2), \hat\Psi^\dagger(\theta_1',\theta_2')] = \delta(\theta_1 - \theta_1')\delta(\theta_2 - \theta_2')$. Following [20], we expand the field operators in momentum eigenstates $\hat\Psi(\theta_1,\theta_2) = \frac{1}{2\pi}\sum_{m,n}\hat c_{m,n}e^{im\theta_1}e^{in\theta_2}$, where $[\hat c_{m,n}, \hat c_{m',n'}^\dagger] = \delta_{m,m'}\delta_{n,n'}$ and $\sum_{m,n}|\hat c_{m,n}|^2 = N$. The Heisenberg equation yields equations of motion for the fields $\hat a_1$, $\hat a_2$, and $\hat c_{m,n}$. For large occupation of the two resonator modes and for the momentum states the field operators can be approximated by complex numbers,

$$\frac{da_1}{dt} = \frac{g\Omega}{2\Delta_a}\sum_{m,n} c_{m,n}^* c_{m-1,n} - i\frac{g^2}{\Delta_a}a_2\sum_{m,n} c_{m,n}^* c_{m-1,n+1} + i\left(\Delta_c - \frac{Ng^2}{\Delta_a}\right)a_1 - \kappa_c a_1, \tag{4a}$$

$$\frac{da_2}{dt} = \frac{g\Omega}{2\Delta_a}\sum_{m,n} c_{m,n}^* c_{m,n-1} - i\frac{g^2}{\Delta_a}a_1\sum_{m,n} c_{m,n}^* c_{m+1,n-1} + i\left(\Delta_c - \frac{Ng^2}{\Delta_a}\right)a_2 - \kappa_c a_2, \tag{4b}$$

$$\begin{aligned}\frac{dc_{mn}}{dt} = &-i(\omega_{r1}m^2 + \omega_{r2}n^2)c_{m,n}\\ &+ \frac{g\Omega}{2\Delta_a}[a_1^* c_{m-1,n} + a_2^* c_{m,n-1} - a_1 c_{m+1,n} - a_2 c_{m,n+1}]\\ &- i\frac{g^2}{\Delta_a}[a_1 a_2^* c_{m+1,n-1} + a_1^* a_2 c_{m-1,n+1}]\\ &+ i\left(\Delta_c - \frac{Ng^2}{\Delta_a}\right)(|a_1|^2 + |a_2|^2)c_{m,n}.\end{aligned} \tag{4c}$$

The amplitudes $c_{m,n}$ of the momentum states are normalized to the total number of atoms in the condensate $\sum|c_n|^2 = N$. Similarly, $|a_1|^2$ and $|a_2|^2$ are the number of photons in the two modes of the cavity. The resonator detuning $\Delta_c = \omega_p - \omega_{\text{TEM00}}$ is defined as the difference of the pump laser frequency and the frequency of the TEM_{00} mode of the empty resonator. The terms containing the decay rate κ_c have been introduced heuristically to describe cavity damping. The last term in Eq. (4c) leads to a phase factor which is the same for all momentum states. It thus can be neglected.

For small pump intensities, the populations of the momentum states change on a time scale much longer than the cavity decay time. In this regime it is possible to adiabatically eliminate the equations for the resonator and derive simple rate equations for the population of the momentum states. Small coupling is achieved for collective Rabi frequencies $\sqrt{N}g\Omega/(2|\Delta_a|) \ll \kappa_c$. For deriving simple rate equations we also neglect the term proportional to g^2. It describes

cross-cavity-mode scattering and comes into play only after many photons have been scattered into the resonator and the light power in the resonator becomes comparable to the power of the pump beam. Rate equations are thus valid only for small photon numbers in the cavity. By substituting $c_{m,n} = \tilde{c}_{m,n} e^{-i(m^2\omega_{r1}+n^2\omega_{r2})t}$ and formally integrating Eqs. (4a) and (4b) one obtains

$$\begin{aligned} a_1(t) &= \frac{g\Omega}{2\Delta_a} \sum_{m,n} e^{-i\omega_{r1}(1-2m)t} \int_0^t dt'\, \tilde{c}^*_{m,n}(t-t')\tilde{c}_{m-1,n}(t-t') \\ &\quad \times e^{[i\omega_{r1}(1-2m)+i\Delta_c-\kappa]t'}, \\ a_2(t) &= \frac{g\Omega}{2\Delta_a} \sum_{m,n} e^{-i\omega_{r2}(1-2n)t} \int_0^t \tilde{c}^*_{m,n}(t-t')\tilde{c}_{m-1,n}(t-t') \\ &\quad \times e^{[i\omega_{r2}(1-2n)+i\Delta_c-\kappa]t'} dt'. \end{aligned} \tag{5}$$

For small pump intensities the amplitudes $\tilde{c}_{i,j}(t)$ vary slowly in time and can thus be shifted outside the integral. The integration can now be carried out analytically. The resulting expressions for the optical fields are substituted in Eq. (4c), and one obtains equations for the populations $N_{m,n} := |\tilde{c}_{m,n}|^2$. By dropping all coherences, i.e., products of the form $\tilde{c}^*_{m,n}\tilde{c}_{m',n'}$ with $m \neq m'$ and $n \neq n'$, one arrives at the rate equations

$$\begin{aligned} \frac{dN_{m,n}}{dt} &= 2\left(\frac{g\Omega}{2\Delta_a}\right)^2 \kappa \left(\frac{N_{m,n}N_{m-1,n}}{[\Delta_c+\omega_{r1}(1-2m)]^2+\kappa^2} \right. \\ &\quad \left. + \frac{N_{m,n}N_{m,n-1}}{[\Delta_c+\omega_{r2}(1-2n)]^2+\kappa^2} \right) \\ &\quad - 2\left(\frac{g\Omega}{2\Delta_a}\right)^2 \kappa \left(\frac{N_{m,n}N_{m+1,n}}{[\Delta_c-\omega_{r1}(1+2m)]^2+\kappa^2} \right. \\ &\quad \left. + \frac{N_{m,n}N_{m,n+1}}{[\Delta_c-\omega_{r2}(1+2n)]^2+\kappa^2} \right). \end{aligned} \tag{6}$$

Each momentum state exchanges populations only with its four neighboring states. The transitions feature Lorentz-shaped resonances with specific resonance frequencies. By controlling the resonator, one can thus individually tune each of the four momentum-transitions into resonance. Furthermore, the transition rate depends not only on the population of the initial state but also on the final state. This can be interpreted as bosonic enhancement due to quantum statistics. Also, note that each momentum state loses population to higher-momentum states and receives population from lower-momentum states. The population thus always flows to higher momentum. Starting with a condensate at rest, there will be no population transferred into states with negative m or n. This is in contrast to the solutions of the full Eq. (4c), which also includes photon scattering from the resonator into the pump beam. Numerical simulations of the rate equations show that the initial population of the resting condensate is shifted to higher-momentum states preferentially as a whole, such that at a given time one typically finds a maximum of two occupied states. This is the result of strong mode competition due to bosonic enhancement: Once a state is slightly more populated than its neighbors, it attracts population with an increasing rate. By tuning the resonator with a proper frequency sequence, it should thus be possible to transfer the condensate into an arbitrary momentum state in a controlled way.

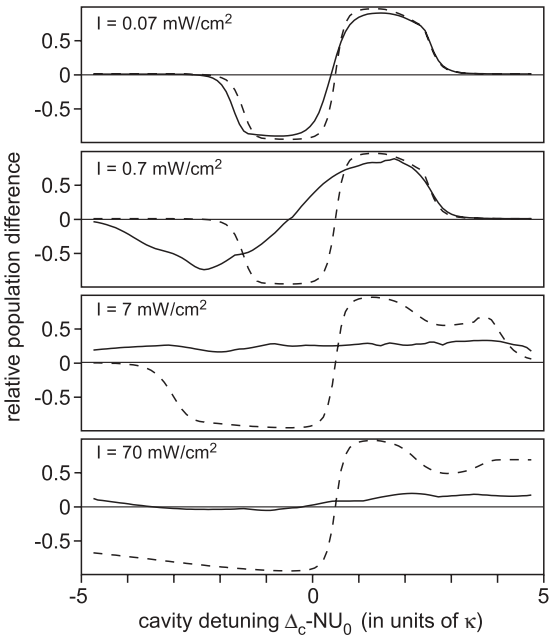

FIG. 4. Maximum possible population difference between the two momentum states with $m = 1$, $n = 0$ and $m = 0$, $n = 1$ for various pump laser detunings $\Delta_c - U_N$ and pump intensities. The solid (dashed) line shows the result of the mean-field (rate) model. Initially, 80 000 atoms are in the zero-momentum state with $m = 0$, $n = 0$. The simulated momentum space is in the range $-2 \leqslant m \leqslant 3$ and $-2 \leqslant n \leqslant 2$. To start the dynamics each finite-momentum state is initially populated with one atom. The initial number of photons in the resonator is set to zero. The dynamics is simulated for 10 ms after the pump beam has been turned on and the maximum population difference within this time interval is plotted. After 10 ms almost all atoms have scattered more than one photon, and only momentum states with $n,m > 1$ are populated.

The rate equations are valid only if the coherences between the momenta can be omitted. This is especially true at the beginning of the dynamics when only one or two momentum states are macroscopically occupied. In fact, simulations of the full Eq. (4c) (without cross-cavity-mode scattering) show that in the limit of small pump power the solutions of the rate equations are reproduced for the low-momentum states. For higher momenta the agreement is only qualitative, and the rate model fails to describe the quantitative details. Nevertheless, for small intensities the full equations also show a lack of scattering back into the pump beam and a clear tendency to transfer the population as a whole. For stronger pumping the addressability of individual transitions by proper tuning of the cavity is gradually lost. This is to be expected when the collective Rabi frequency exceeds the cavity linewidth such that power broadening reduces the cavity resolution. The fast dynamics of the populations then increases the frequency uncertainty of the momentum states beyond the resolution of the resonator. To show this effect we plot the maximum population difference that can be reached for the momentum states $|m = 1,n = 0\rangle$ and $|m = 0,n = 1\rangle$ for various detunings and intensities (see Fig. 4). For small pump intensities, the rate model and the full model reasonably agree, and the population difference shows a clear sensitivity to the cavity detuning. According to the full equations, the frequency sensitivity is

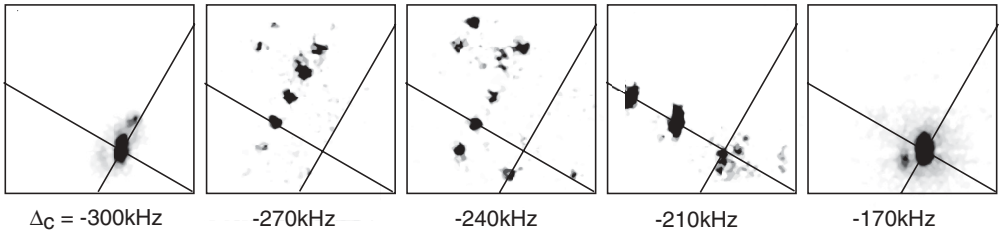

FIG. 5. Time-of-flight absorption images for various pump laser detunings Δ_c. The pump duration was 200 μs with a pump beam intensity of $I_p = 50$ mW/cm^2 and an atomic detuning of $\Delta_a = -2\pi \times 4.7$ GHz. The solid lines indicate the positions of states with $m = 0$ and $n = 0$.

lost for higher intensities. The rate model fails to describe this effect correctly.

IV. OBSERVATIONS

Figure 5 shows absorption images for various pump laser detunings, 200 μs after the pump laser has been turned on. For a pump intensity of $I = 50$ mW/cm^2 and an atomic detuning of $\Delta_a = -2\pi \times 4.7$ GHz, the coupling is strong, and the rate model does not hold. Nevertheless, a detuning by a few κ_c still substantially changes the momentum pattern. Each momentum state scatters pump light into the cavity with an individual recoil shift. If the scattered light is in resonance with the cavity, the scattering process is enhanced or otherwise suppressed. Furthermore, the oblique angle of incidence of the pump light lifts the degeneracy between the two counterpropagating cavity modes. Depending on the detuning, the light is thus preferentially scattered in one of the two cavity modes. Scattering from higher-momentum states suffers from large recoil shifts and is eventually disrupted. Note that for detunings of -270 and -240 kHz, backscattering into the pump beam gives rise to a momentum state with negative m and n. For negative detuning from the atomic resonance, $\Delta_a < 0$, the cavity detuning for which scattering is observed is also negative, $\Delta_c < 0$. As discussed in Ref. [13], the refractive index of the atomic cloud shifts the resonance frequency of the cavity modes by the amount $NU_0 = Ng^2/\Delta_a$. However, the experimentally observed detuning on the order of 200 kHz is surprisingly large and cannot be fully explained by condensed and thermal atoms which occupy the cavity-mode volume. Here, one can speculate to what extent the finite size of the atomic cloud plays a role. Also, recently discussed Mie resonances [21] may be important.

For comparison with theory we restrict ourselves to the low-lying momentum states $|m,n\rangle = |0,0\rangle$, $|1,0\rangle$, $|2,0\rangle$, and $|1,1\rangle$. The dots in Fig. 6 show the observed relative occupation of the four selected momentum states for various pump durations. In total 21 absorption images have been recorded for various pump duration times, and the relative occupation numbers have been derived. The data have been binned in time intervals of 10 μs and averaged over each bin. Because of the background in the absorption images, the population numbers can be determined only with an error of several tens of percent. Nevertheless, one can clearly see that the populations evolve in time from the original state $|0,0\rangle$ via $|1,0\rangle$ toward $|2,0\rangle$, with a small portion being transferred to the state $|1,1\rangle$. The predictions of the full equations and of the rate model are shown as solid and dashed lines. The agreement with the mean field is not perfect but is reasonable. As discussed in Sec. III, the rate model predicts a population transfer as a whole, a behavior which is clearly not observed in the experiment. The simulations are very sensitive to the initial atom numbers in the momentum states and photon numbers in the resonator. The atom number is determined by calculating the thermal population of the discrete momentum states with

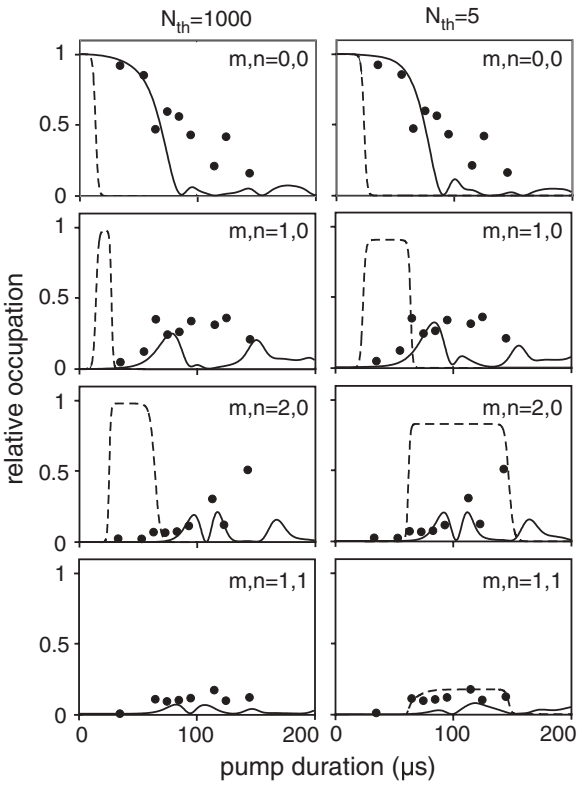

FIG. 6. Population of selected momentum states (m,n) for various pump durations. The pump intensity amounts to $I = 70$ mW/ cm^2, the detuning of the pump frequency from the atomic resonance is $\Delta_a = 2\pi \times 4.3$ GHz, and the detuning from the cavity mode is $\Delta_c = 2\pi \times 253$ kHz. The solid (dashed) line presents the prediction of the mean-field (rate) model for an initial atom number of $N = 80\,000$ in the condensate. The finite-momentum states are initially occupied with $N_{\rm th} = 1000$ and $N_{\rm th} = 5$ thermal atoms distributed over the discrete-momentum states according to Bose-Einstein statistics. The initial condition for the cavity field is $a_1 = a_2 = 5$, corresponding to 25 photons in each of the two modes. The simulated momentum space is in the range $-2 \leqslant m \leqslant 3$ and $-2 \leqslant n \leqslant 2$. In the simulations the cavity detuning has been set to $\Delta_c - NU_0 = 2\kappa$.

a Bose-Einstein statistics for a quantum gas below the critical temperature for condensation. In this regime, the only free parameter is the number of thermal atoms $N_{\rm th}$ distributed over the discrete momentum states. It cannot be determined experimentally with good accuracy and has to be estimated. In Fig. 6 simulations are plotted for $N_{\rm th} = 5$ and $N_{\rm th} = 1000$. While the rate model gives substantially different results for the two numbers, the mean-field model is not very affected. However, it is very sensitive to the initial photon number, which obviously plays no role in the rate model. Here, the best agreement with the observation is obtained with 25 initial photons in each of the two cavity modes. The assumption of some initial photons in the cavity is reasonable since stray light from the windows of the vacuum chamber and other optical elements may hit the cavity mirrors, which then scatter the light into the cavity modes. The Purcell effect also enhances this kind of unwanted scattering.

The intensity dependence of the atomic population after a pump duration of 200 μs is shown in Fig. 7. In total 12 absorption images have been recorded for various intensities,

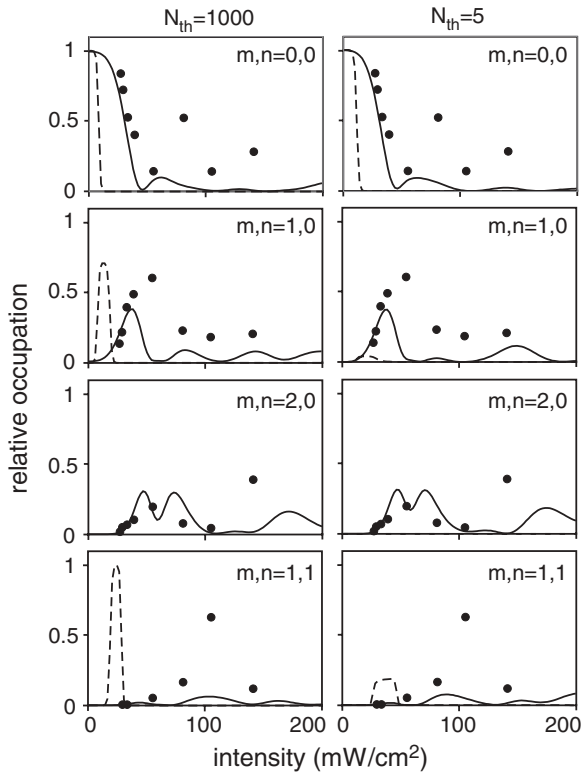

FIG. 7. Relative population of selected momentum states (m,n) for various pump beam intensities I. The pulse duration is 200 μs, and the detuning from the atomic resonance $\Delta_a = -2\pi \times 8.4$ GHz. The laser is resonant to the empty cavity mode, $\Delta_c = 0$. The solid (dashed) line presents the prediction of the semiclassical (rate) model for an initial atom number of $N = 80\,000$ in the condensate. The finite-momentum states are initially occupied with $N_{\rm th} = 1000$ and $N_{\rm th} = 5$ thermal atoms outside the condensate distributed over the discrete-momentum states according to Bose-Einstein statistics. The initial condition for the cavity field is $a_1 = a_2 = 5$, corresponding to 25 photons in each of the two modes. The simulated momentum space is in the range $-2 \leqslant m \leqslant 3$ and $-2 \leqslant n \leqslant 2$. The effective cavity detuning has been set to $\Delta_c - NU_0 = 0.8\kappa$.

and the relative occupation numbers have been derived. Again, the typical error amounts to 50%, particularly for small occupation numbers. The predictions of the full equations and of the rate model are shown as solid and dashed lines. With increasing intensity, population is transferred to higher-momentum states. Again, the rate model drastically fails to describe the data, while agreement with the mean-field model is reasonable.

V. DISCUSSION AND OUTLOOK

The experiments presented in this paper are performed in the regime of strong pumping, where the collective Rabi frequency exceeds the cavity linewidth. The frequency selectivity of the cavity is thus limited and cannot be efficiently exploited to control the dynamics of the atom-light interaction. The nonadiabatic response of the cavity leads to a complex dynamics with irregular oscillatory exchange of energy between light and atoms. This dynamics can be well described with a mean-field quantum model but not with a rate-equation model. The experimental data are noisy; however, a better data quality requires substantial improvement of the apparatus. Since the atoms spread out over many momentum states, the atom number per state is small and difficult to observe in the absorption images against the background noise. An exact determination of the atom number is also required to control the detuning of the cavity due to the atomic index of refraction. The simulations show a strong sensitivity to the initial conditions. In fact, if all technical noise can be suppressed and only quantum fluctuations remain, the dynamical instability can be interpreted as a quantum phase transition. This strictly holds only for a homogeneous quantum gas and plane light waves. In the experiment, however, we have to deal with localized resonator modes and cigar-shaped condensates. While in a homogeneous gas any other but forward scattering is triggered by fluctuations only, a finite gas exhibits Mie-type scattering in many directions [21–23]. For the future, it will thus be very interesting to understand how Mie-type scattering triggers the instability and potentially covers the quantum phase transition. Resonant photons deposited inside the condensate by light-induced collisions may also be of some importance [19]. Beyond triggering phase transitions, there is also a general interest in collective scattering from a finite atomic cloud [24–26].

Regardless of how exactly the instability is triggered, it nevertheless allows us to stably prepare the atoms in an unconventional superfluid quantum state with finite momentum provided that the light scattering stops for higher-momentum states. This is possible in the rate-equation regime, where the frequency sensitivity of the cavity is fully developed. For higher-momentum states the recoil shift exceeds the cavity linewidth, and the scattered light is no longer resonant with the cavity. The dynamic stops and the system relaxes into a metastable state with no light in the cavity and the atoms in a superfluid state of finite momentum. Since the required dissipation is provided by the cavity and its limited linewidth, the process resembles scenarios in which the atoms are transferred into low-energy states with cavity cooling [27]. For weak pumping the full equations are well approximated by the rate-equation model. In this regime, the decay into a

high-momentum state can thus be interpreted as a consequence of mode competition due to bosonic enhancement.

A similar picture also applies to a recently proposed scenario for investigating Dicke-type subradiance [14]: Scattering from the zero-momentum state into a target state of finite momentum is inhibited by means of a second pump laser. It depletes any population from the target state and, by this, suppresses any bosonic enhancement. The remaining spontaneous rate is orders of magnitude smaller and can be neglected. This effect is closely related to Dicke subradiance [28,29], a phenomenon which is barely investigated experimentally with atomic clouds [30,31].

The rate-equation regime can be reached for reduced light intensities (<1 mW/cm^2) and consequently longer pump durations beyond 1 ms. At this time scale, collisions between the atoms begin to play a role. The momentum states imprinted on the condensate during light scattering correspond to velocities higher than the critical velocity for superfluidity. The atomic motion is particle-like, and scattering between the atoms may lead to heating. It remains to be seen to what extent the coherence of the condensate wave function is affected.

In summary, we have analyzed a recent experiment on cavity-assisted light scattering from a Bose-Einstein condensate. From a mean-field description of the atomic matter field, a rate-equation model has been derived by adiabatic elimination of the light field. The experiment has been carried out in the strong-pumping regime and can be described by the mean-field model with reasonable agreement. The rate-equation model approximately holds in the weak-pumping regime, where the time scale of the atomic motion exceeds the cavity decay time. In this regime the spectral resolution of the resonator is fully developed and can be used to study novel effects such as unconventional superfluidity and Dicke subradiance.

ACKNOWLEDGMENTS

This work has been supported by the Deutsche Forschungsgemeinschaft and the Research Executive Agency (program COSCALI, Grant No. PIRSES GA-2010-268717). S.B. acknowledges support from the Carl-Zeiss-Stiftung. H.T. acknowledges support from the Evangelisches Studienwerk in Villigst.

[1] A. T. Black, H. W. Chan, and V. Vuletic, Phys. Rev. Lett. **91**, 203001 (2003).
[2] B. Nagorny, Th. Elsässer, and A. Hemmerich, Phys. Rev. Lett. **91**, 153003 (2003).
[3] D. Kruse, Ch. von Cube, C. Zimmermann, and Ph. W. Courteille, Phys. Rev. Lett. **91**, 183601 (2003).
[4] S. Slama, S. Bux, G. Krenz, C. Zimmermann, and Ph. W. Courteille, Phys. Rev. Lett. **98**, 053603 (2007); S. Slama, G. Krenz, S. Bux, C. Zimmermann, and Ph. W. Courteille, Phys. Rev. A **75**, 063620 (2007).
[5] K. Baumann, R. Mottl, F. Brennecke, and T. Esslinger, Phys. Rev. Lett. **107**, 140402 (2011).
[6] M. Wolke, J. Klinner, H. Keßler, and A. Hemmerich, Science **337**, 85 (2012).
[7] Ph. W. Courteille, in *Long-Range Interacting Systems*, Lecture Notes of the Les Houches Summer School Vol. 90 (Oxford University Press, Oxford, 2009), p. 505
[8] R. Mottl, F. Brennecke, K. Baumann, R. Landig, T. Donner, and T. Esslinger, Science **336**, 1570 (2012).
[9] R. Bonifacio, L. De Salvo Souza, Nucl. Instrum. Methods Phys. Res., Sect. A **341**, 360 (1994); N. Piovella, M. Gatelli, and R. Bonifacio, Opt. Commun. **194**, 167 (2001).
[10] I. B. Mekhov, C. Maschler, and H. Ritsch, Phys. Rev. Lett. **98**, 100402 (2007).
[11] M. H. Schleier-Smith, I. D. Leroux, H. Zhang, M. A. Van Camp, and V. Vuletic, Phys. Rev. Lett. **107**, 143005 (2011).
[12] K. Baumann, C. Guerlin, F. Brennecke, and T. Esslinger, Nature (London) **464**, 1301 (2010).
[13] S. Bux, Ch. Gnahm, R. A. W. Maier, C. Zimmermann, and Ph. W. Courteille, Phys. Rev. Lett. **106**, 203601 (2011).
[14] M. M. Cola, D. Bigerni, and N. Piovella, Phys. Rev. A **79**, 053622 (2009).
[15] S. Inouye, A. P. Chikkatur, D. M. Stamper-Kurn, J. Stenger, D. E. Pritchard, and W. Ketterle, Science **285**, 571 (1999).
[16] M. Kozuma, Y. Suzuki, Y. Torii, T. Sugiura, T. Kuga, E. W. Hagley, and L. Deng, Science **286**, 2309 (1999).
[17] H. Tanji-Suzuki, I. D. Leroux, M. H. Schleier-Smith, M. Cetina, A. T. Grier, J. Simon, and V. Vuletic, Adv. At. Mol. Opt. Phys. **60**, 201 (2011).
[18] S. Bux, G. Krenz, S. Slama, C. Zimmermann, and Ph. W. Courteille, Appl. Phys. B **89**, 181 (2007).
[19] N. S. Kampel, A. Griesmaier, M. P. Hornbak Stenstrup, F. Kaminski, E. S. Polzik, and J. H. Müller, Phys. Rev. Lett. **108**, 090401 (2012).
[20] N. Piovella, Eur. Phys. J. Spec. Top. **203**, 127 (2012).
[21] R. Bachelard, H. Bender, P. W. Courteille, N. Piovella, C. Stehle, C. Zimmermann, and S. Slama, Phys. Rev. A **86**, 043605 (2012).
[22] M. O. Scully, E. S. Fry, C. H. R. Ooi, and K. Wódkiewicz, Phys. Rev. Lett. **96**, 010501 (2006).
[23] Ph. W. Courteille *et al.*, Eur. Phys. J. D **58**, 69 (2010).
[24] S. Bux, E. Lucioni, H. Bender, T. Bienaimé, K. Lauber, C. Stehle, C. Zimmermann, S. Slama, Ph. W. Courteille, N. Piovella, and R. Kaiser, J. Mod. Opt. **57**, 1841 (2010).
[25] T. Bienaimé, S. Bux, E. Lucioni, Ph. W. Courteille, N. Piovella, and R. Kaiser, Phys. Rev. Lett. **104**, 183602 (2010).
[26] H. Bender, C. Stehle, S. Slama, R. Kaiser, N. Piovella, C. Zimmermann, and Ph. W. Courteille, Phys. Rev. A **82**, 011404(R) (2010).
[27] V. Vuletic, H. W. Chan, and A. T. Black, Phys. Rev. A **64**, 033405 (2001).
[28] R. H. Dicke, Phys. Rev. **93**, 99 (1954).
[29] A. Crubellier and D. Pavolini, J. Phys. B **20**, 1451 (1987).
[30] D. Pavolini, A. Crubellier, P. Pillet, L. Cabaret, and S. Liberman, Phys. Rev. Lett **54**, 1917 (1985).
[31] N. Cui, M. Macovei, K. Z. Hatsagortsyan, and C. H. Keitel, Phys. Rev. Lett **108**, 243401 (2012).